

Journal of Mechanics of Materials and Structures

**DYNAMICS OF FRP STRENGTHENED UNIDIRECTIONAL MASONRY WALLS
II: EXPERIMENTS AND COMPARISON**

Oded Rabinovitch and Hazem Madah

Volume 7, No. 1

January 2012

DYNAMICS OF FRP STRENGTHENED UNIDIRECTIONAL MASONRY WALLS II: EXPERIMENTS AND COMPARISON

ODED RABINOVITCH AND HAZEM MADAH

In this part of the paper, the dynamic out-of-plane behavior of a unidirectional strengthened masonry wall is studied experimentally. The experimental phase focuses on shake-table testing of a full-scale masonry wall strengthened with carbon fiber reinforced composite strips. The tested wall is subjected to different combinations of in-plane compression and out-of-plane excitation. The dynamic behavior of the wall is monitored with emphasis on the global out-of-plane displacements and accelerations as well as on the localized displacements and strains near the mortar joints. The experimental results are also used for the assessment of the finite element model developed in part I of the paper. The experimental results, the numerical analysis, and the comparison between the two throw light on the global and local aspects of the dynamic response. The numerical model allows for further study of local-scale results, which cannot be monitored experimentally. In particular, the dynamics of the shear and peeling stresses at the adhesive layers are examined. The comparison of the experimental results with ones obtained for the same wall before strengthening demonstrate the potential of the method and its impact on the dynamics of the masonry wall.

1. Introduction

Masonry walls are a structural form that can be found in almost every building around the world. Masonry construction characterizes many historic buildings but it still serves as a building technique widely used as infill walls in modern structural systems. Along with its many advantages, the unique characteristics of the masonry construction make the masonry wall vulnerable to out-of-plane static and mainly dynamic loads. For example, in [Rabinovitch and Madah 2011] we experimentally and analytically examined the behavior of unreinforced masonry walls under out-of-plane dynamic loads. The experimental observations reflected the limited ability of the wall to resist such loads and the impact of the boundary conditions and the level of in-plane compression on this limited ability. The tendency of the boundary conditions and the in-plane loading conditions to unfavorably change during a dynamic loading may lead to a severe degradation in the structural performance and to a potential collapse of the wall. In case of a seismic event, this type of behavior may endanger the occupants, even if the main structural skeleton is intact [Flanagan and Bennett 1999; Wu et al. 2005; Meisl et al. 2007].

The above observations highlight the need to strengthen the masonry wall, not only to resist in-plane loads but also to resist out-of-plane ones. The use of externally bonded composites is an excellent solution for this need [Albert et al. 2001; Hamilton and Dolan 2001; Griffith et al. 2004; Gilstrap and Dolan 1998]. The addition of a strong, stiff, lightweight, and durable externally bonded tensile resisting layer provides

This research was supported by The Israel Science Foundation, Grant No. 772/06.

Keywords: masonry wall, composite material, dynamic behavior, shake table experiments, strengthening.

the wall with a supplemental load resisting mechanism and with the ability to resist out-of-plane loads through flexure. This ability was demonstrated in various experimental programs that examined the static out-of-plane response of the strengthened wall [Albert et al. 2001; Hamilton and Dolan 2001; Griffith et al. 2004; Gilstrap and Dolan 1998; Hamed and Rabinovitch 2010a; Hamed and Rabinovitch 2010b]. The more important challenge is, however, to examine, characterize, and demonstrate the response of the strengthened wall to dynamic loads.

The dynamic behavior of masonry walls strengthened with externally bonded composite materials has been the subject of various experimental studies reported in the past decade, such as [ElGawady et al. 2002; 2003; Turek et al. 2007; El-Dakhkhni et al. 2004; Almusallam and Al-Salloum 2007; Altin et al. 2008]. These studies mainly focused on the in-plane response of the wall. The number of works that experimentally studied the dynamic out-of-plane response is much smaller. Among them, [Davidson et al. 2005] and [Myers et al. 2004] examined the out-of-plane dynamic response of masonry wall sprayed with polymeric layers to blast loads. The dynamic characteristics of these loads and, correspondingly, the strengthening technique, are different from the ones associated with the response to seismic or wind loads studied here.

Al-Chaar and Hasan [2002] studied the coupled and the out-of-plane response of masonry walls rehabilitated with composite overlays and subjected to uniaxial and triaxial dynamic excitation. The results showed that the composite overlay enhances the seismic resistance of the masonry wall by increasing its ultimate strength and modifying its dynamic properties by about 25–40%. On the other hand, it was observed that cracking and the nonlinear behavior of the wall couples the dominant frequencies and the level of damage (also see [Carpinteri and Pugno 2005; Thompson and Stewart 1986]). These important observations are mainly focused on the global-scale response of the wall. Further attention should be drawn to localized effects, which are critical for the understanding of the behavior of the structure and for the assessment of analytical or numerical models.

The objectives of this paper are to experimentally study the out-of-plane dynamic behavior of unidirectional strengthened masonry wall panels and to comparatively assess the FE model developed in part I [Rabinovitch and Madah 2012]. To achieve these goals, a full-scale unidirectional masonry wall that is strengthened with externally bonded strips made of carbon fiber reinforced polymer (CFRP) is tested under out-of-plane dynamic excitation. The shake table test setup follows the one used in [Rabinovitch and Madah 2011] for unreinforced unidirectional masonry walls. The results of the shake-table experiments and the comparison with the response of the same wall tested before strengthening (*loc. cit.*) are used in order to gain insight into the characteristics of the dynamic response. In addition, they are used for a critical evaluation and possible support of the numerical model developed in part I. With that in mind, additional results that cannot be directly detected experimentally but can be obtained through the numerical model, are presented and discussed. Emphasis is placed on the interfacial effects, on the stress concentrations near irregular points, and on their variation in time during the dynamic loading event.

The paper is organized as follows. The experimental setup, the material properties and characterization, and the finite element model are presented first. Then the experimental results of two tests that differ in the level of axial loading applied during the dynamic excitation are presented and discussed. The first set of results obtained under the higher level of axial loading is compared with the results of the FE analysis. The second set is compared with the response of the wall before strengthening [Rabinovitch and Madah

2011] with emphasis on the impact of the strengthening system on the dynamic response of the wall. The paper closes with a summary and conclusions.

2. Shake-table experiments and FE analysis

2.1. Test setup. The shake-table test setup follows the one reported in [Rabinovitch and Madah 2011] for testing the unstrengthened wall. For completeness, it is presented here. The shake table apparatus is illustrated in Figure 1. The wall is excited in its out-of-plane direction and therefore is it built inside a steel frame that is mounted on the shake table facing the direction of the motion (see Figure 1c). The steel frame is mounted on the table and rigidly supported at its top. The upper supporting point is connected to the shake table using the triangular steel construction shown in Figure 1c. This configuration yields a coordinated and controlled movement of the top and bottom of the wall. These conditions are designed to avoid interstorey drift and relative movement of the top of the wall with respect to its bottom. The wall is sandwiched between two concrete elements (beams) that simulate the lower and upper slabs. On

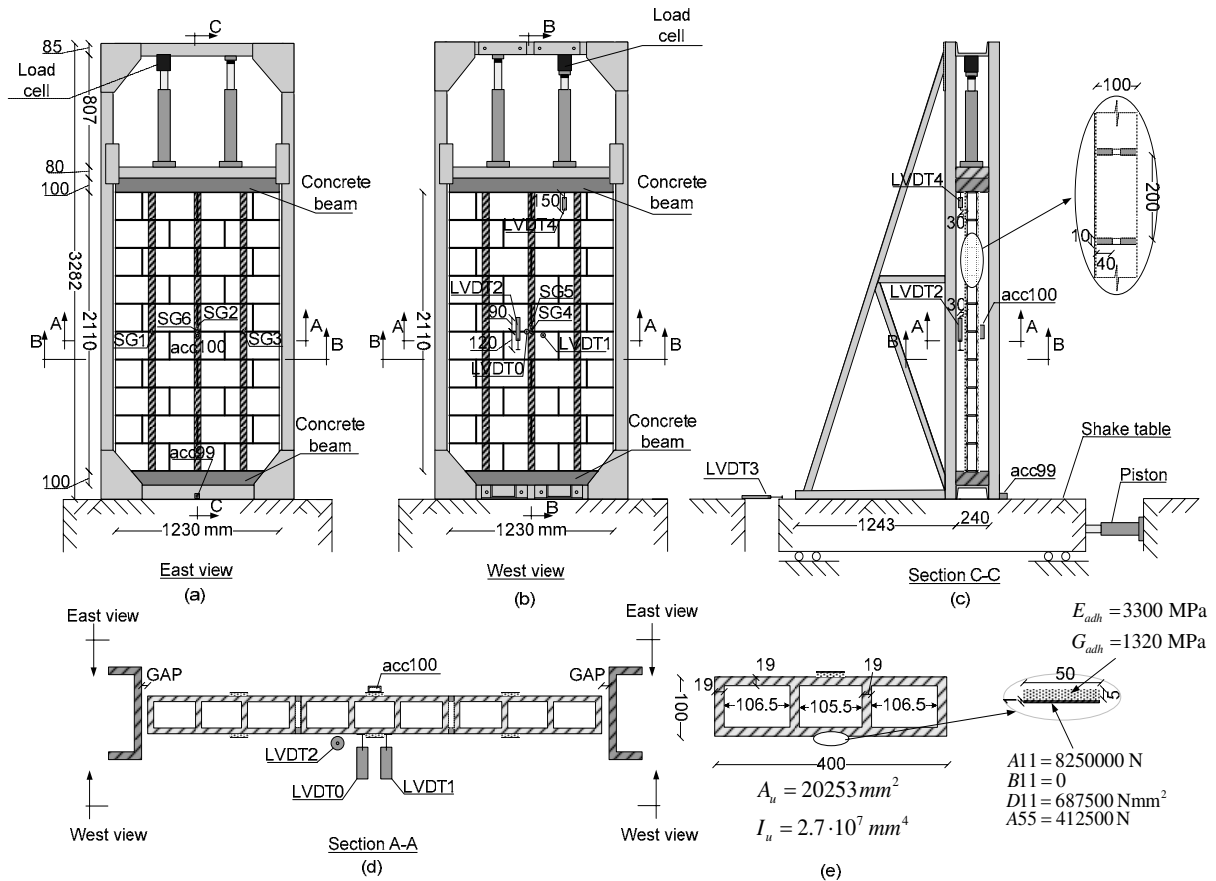


Figure 1. Dynamic test setup (dimensions in mm). (a) east view; (b) west view; (c) section C-C; (d) section A-A; (e) geometry and properties of the masonry unit, FRP strips, and adhesive layers.

the other hand, the wall is disconnected from the columns of the steel frame yielding a unidirectional out-of-plane flexural scheme and transfer of loads in the height direction only.

The simulation of the gravity load transferred to the wall from the upper slab is achieved using two hydraulic jacks (Figure 1a-c). The axial compression applied by the jacks also controls the level of cracking in the wall. The detail at the top of the wall restricts the lateral (out-of-plane) displacement and the rotation of the upper concrete beam but allows the beam to move in the vertical direction. This allows transferring the in-plane compressive load to the tested wall. It should, however, be noted that the preliminary testing has shown that the hydraulic system at the top of the wall (the two jacks and the hydraulic fluid lines) has a certain level of vertical compliance, which has to be taken into account. Along with the vertical load, the entire apparatus, which includes the shake table, the supporting steel frame, the wall, and the axial loading system at its top, are excited dynamically. The control system is based on closed loop dynamic controller.

The tested wall is built of 400/200/100 hollow concrete units. The cross section of the wall and the general layout of the masonry assembly are shown in Figure 1d,e. The masonry units are connected through mortar head and bed joints. Following conventional masonry building techniques, the mortar in the bed joints is applied in two strips on top of the masonry unit's outer shells. The width of each strip is about 400 mm and the thickness of the bed joints is about 10 mm. The thickness of the head joints is also about 10 mm. The overall dimensions of the tested wall are about 1230 by 2110 mm.

The wall was dynamically tested prior to strengthening. The results of this initial testing phase are reported in [Rabinovitch and Madah 2011]. At the initial phase of testing, the wall was subjected to different combinations of axial loading and out of plane dynamic excitation. Testing under 2800 N and a cyclic excitation with frequency of 8.3 Hz and amplitude of about ± 1 mm yielded extensive cracking at the middle joint and brought the wall close to collapse (see [Rabinovitch and Madah 2011] for more details).

After the initial dynamic loading, the wall was strengthened using six externally bonded CFRP strips, three on each face. The configuration of the CFRP strips is shown in Figure 1. Before strengthening, the wall's surface was cleaned and a preliminary layer of epoxy was applied on the wall's surface. After the primer layer was cured, the CFRP strips were installed in place. The strips were not mechanically fastened or anchored at the edges, at the supporting frame, or at any other point. The final thickness of the adhesive equals about 5 mm.

The monitoring devices include five LVDTs, two accelerometers, one load cell, and six stain gauges. The various devices and their locations are illustrated in Figure 1. The out of plane displacements (relative to the surrounding frame) are monitored by LVDT0 and LVDT1. The crack opening across the middle bed joint and the crack opening between the upper masonry unit and the upper concrete element are detected by LVDT2 and LVDT4, respectively. The absolute displacement of the shake-table is monitored by LVDT3. The out-of-plane acceleration at the shake-table level and the out-of-plane acceleration at the middle of the wall are monitored by the two accelerometers (acc 99, and acc 100, respectively). The compressive load applied by the hydraulic system at the top of the wall and its temporal variation are dynamically monitored by the load cell.

The six strain gauges are bonded on the outer faces of the FRP strips in two groups. SG1, SG3, and SG6 are bonded on the three FRP strips mounted on the east face of the wall. These strain gauges are bonded across the middle-joint. SG2, on the other hand, is bonded on the middle strip on that

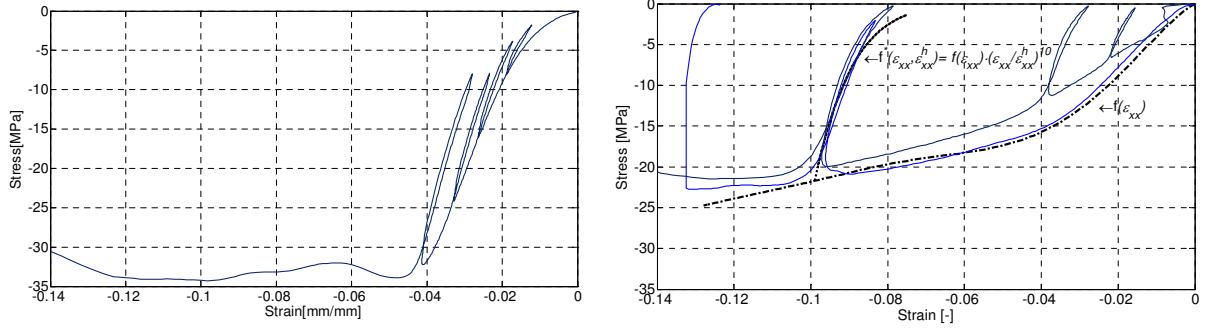


Figure 2. Constitutive relations for the masonry materials. (a) masonry shells; (b) mortar. Legend: — experimental; - - - loading; ····· unloading/reloading.

face but about 30 millimeters above the joint. Similarly, SG4 and SG5 are bonded on the middle strip mounted on the west face of the wall across and above the joint, respectively. All sensors are sampled at 300 samples/sec.

2.2. Material properties. The equivalent elastic modulus of the FRP strips $E^{\text{FRP}} = 165$ GPa and its specific mass $\rho^{\text{FRP}} = 1400$ kg/m³ are based on the data provided by the manufacturer. The shear modulus of the FRP strip is estimated as 8.25 GPa and the shear correction factor is taken as 5/6. The elastic and shear moduli of the adhesive layer follow [Hamed and Rabinovitch 2010a; Hamed and Rabinovitch 2010b] and equal $E = 3.3$ GPa and $G = 1.32$ GPa. Its specific mass is taken as 1070 kg/m³.

The elastic / mechanical properties of the masonry units are estimated based on monotonic and cyclic compressive tests of square 80 by 80 mm specimens cut out from the masonry shell. Some of the results appear in Figure 2a and reveal an approximately linear range running from about 20% up to about 85% of the ultimate load with minor inelastic effects due to unloading / reloading in this range. The crushing strength of the masonry shells is larger than 30 MPa. The average elastic modulus in the quasilinear range equals about 1100 MPa. These observations support the assumption of linear elastic behavior of the masonry unit used in [Rabinovitch and Madah 2012]. The shear modulus of the masonry unit is taken as 440 MPa and its mass density equals 1930 kg/m³. The shear correction factor for the masonry unit cross section is estimated using a 2D finite element analysis and taken as 0.675.

The mortar is made with cement-sand-lime ratio = 1:3:1 and its mass density is about 2400 kg/m³. The constitutive behavior of the mortar under cyclic uniaxial compression is determined experimentally. A characteristic result appears in Figure 2b (also see [Rabinovitch and Madah 2011]). The loading ($f(\epsilon_{xx})$) and the unloading/reloading ($f^*(\epsilon_{xx}, \epsilon_{xx}^h)$) branches are approximated as follows (*loc. cit.*):

$$f(\epsilon_{xx}) = 314\epsilon_{xx} - 0.198 \cdot 10^5 \epsilon_{xx}^2 - 0.706 \cdot 10^6 \epsilon_{xx}^3 - 0.9 \cdot 10^7 \epsilon_{xx}^4 - 0.5 \cdot 10^8 \epsilon_{xx}^5 - 0.1 \cdot 10^9 \epsilon_{xx}^6 \text{ [MPa]}, \quad (1)$$

$$f^*(\epsilon_{xx}, \epsilon_{xx}^h) = f(\epsilon_{xx}^h) \cdot (\epsilon_{xx} / \epsilon_{xx}^h)^{10} \text{ [MPa]}. \quad (2)$$

The shear response of the compressed mortar, $s(\gamma_{xz})$, is assumed linear elastic with a shear modulus $G_j = 166$ MPa ([Hamed and Rabinovitch 2010a; Hamed and Rabinovitch 2010b]). The initial tangent moduli of the mortar material are taken as $E_j = f_{,\epsilon}(\epsilon_{xx} = 0^-) = 314$ MPa and $G_j = s_{,\gamma}(\gamma_{xz} = 0) = 166$ MPa.

2.3. Testing protocol. Following the observations and the data gained from testing of the unstrengthened wall [Rabinovitch and Madah 2011], the wall reported here is tested under a cyclic out-of-plane excitation with frequency of about 8.3 Hz and amplitudes of about ± 1 mm. The application of this dynamic load and vertical loading of about 5000 N (2500 N in each jack) did not bring the unstrengthened wall to failure [Rabinovitch and Madah 2011]. On the other hand, the same dynamic protocol applied to the unstrengthened wall under vertical loading of 2800 N triggered extensive cracking at mid-height. Based on these observations, and in order to compare the results with the behavior of the wall before strengthening, the same two test protocols (i.e., [8.3 Hz, ± 1 mm, 5000 N], [8.3 Hz, ± 1 mm, 2800 N]) are examined here as well.

2.4. Finite element modeling. Two finite element models are examined. Following part I of the paper [Rabinovitch and Madah 2012], both model refer to a characteristic 400 mm wide unidirectional strip. The first model refers to the entire height of the wall. In order to allow analysis with a refined mesh and yet to keep the computational burden reasonable, the second model takes advantage of the out-of-plane symmetry and refers to half of the wall with symmetry conditions. The entire wall is strengthened with 3 strips on each face, therefore the 400 mm wide characteristic strip includes one FRP strip on each face. The full-height model of the characteristic strip includes 10 masonry units, 11 bed joints, and the upper and lower beams, which are assumed linear elastic with $E = 30$ GPa, $G = 12$ GPa, $\rho = 2400$ kg/m³, and a solid cross section. The boundary conditions are applied at the ends of the lower and the upper supporting beams. The lower beam is clamped. The upper beam is free to move in the vertical (axial) direction but its rotation and out-of-plane displacement are constrained. In the vertical direction, the top of the beam is connected to a precompressed spring that simulates the applied load, the weight of the devices at the top of the wall (distributing beam, hydraulic jacks, load cells, etc), and the compliance of the hydraulic loading system. The spring constant is roughly estimated as 1000 kN/m for the examined 400 mm wide strip.

In the symmetric model, the boundary conditions at the bottom of the wall are replaced with sliding clamps at the middle of the mid-height joint. The sliding clamp conditions (free out-of plane displacement, fixed rotation and in-plane displacement) are applied to the masonry wall and the FRP strips. The conditions at the adhesive layers allow free out-of-plane displacement. Note that these conditions violate the lack of symmetry due to the in-plane configuration and the self-weight of the wall. In addition, the symmetric model cannot capture the antisymmetric out-of-plane modes.

The full-height FE mesh includes 502 elements through the height of the wall. Each joint is divided into 2 elements and each masonry unit is divided into 40 elements. The total number of DOFs is 5533. In part I of this paper it has been shown that this type of mesh provides an adequate assessment of the global response but only a rough estimate of the stress concentrations near the joints. For that purpose, the symmetric model uses a refined mesh with 4 elements through the height of the joint and 80 elements through the height of each masonry unit. The dynamic load for both models uses the reading of the accelerometer mounted on the shake-table as a ground acceleration signal. Along with the dynamic excitation, the models are also subjected to the self-weight of the wall, the weight of the loading devices at the top of the wall, and the vertical precompression load. Based on the preliminary convergence study outlined in part I of this paper, the time step of the numerical analysis equals $0.833 \cdot 10^{-3}$ sec. To meet this time step, linear interpolation of the recorded ground acceleration input signal is used. The

proportionality constants for the damping model are calibrated for assumed damping ratios of about 7% in the two first linear modes.

3. Results, comparison, and discussion

The results for the wall vertically loaded to 5000 N (2150 N per the examined 400 mm wide strip, including the added weight at the top of the wall) are presented first. The experimental results and their numerical counterparts are followed by complementary results that cannot be detected experimentally but can be obtained by the numerical analysis. Finally, the results per the wall vertically loaded to 2800 N (1430 N per the examined strip, including added weight) are presented and compared with the ones obtained per the unstrengthened wall under similar dynamic loading conditions.

3.1. Test and analysis results: higher level of vertical loading. The out-of-plane displacements and accelerations detected at the middle of the wall in the experiment, the analysis with the full-height model, and the analysis with the symmetric model are studied in Figure 3. Part (a) of the figure and the zoom plot in (b) reveal displacements in the order of ± 0.4 mm. For comparison, the testing of the wall under the same conditions but before strengthening revealed similar levels of accelerations but

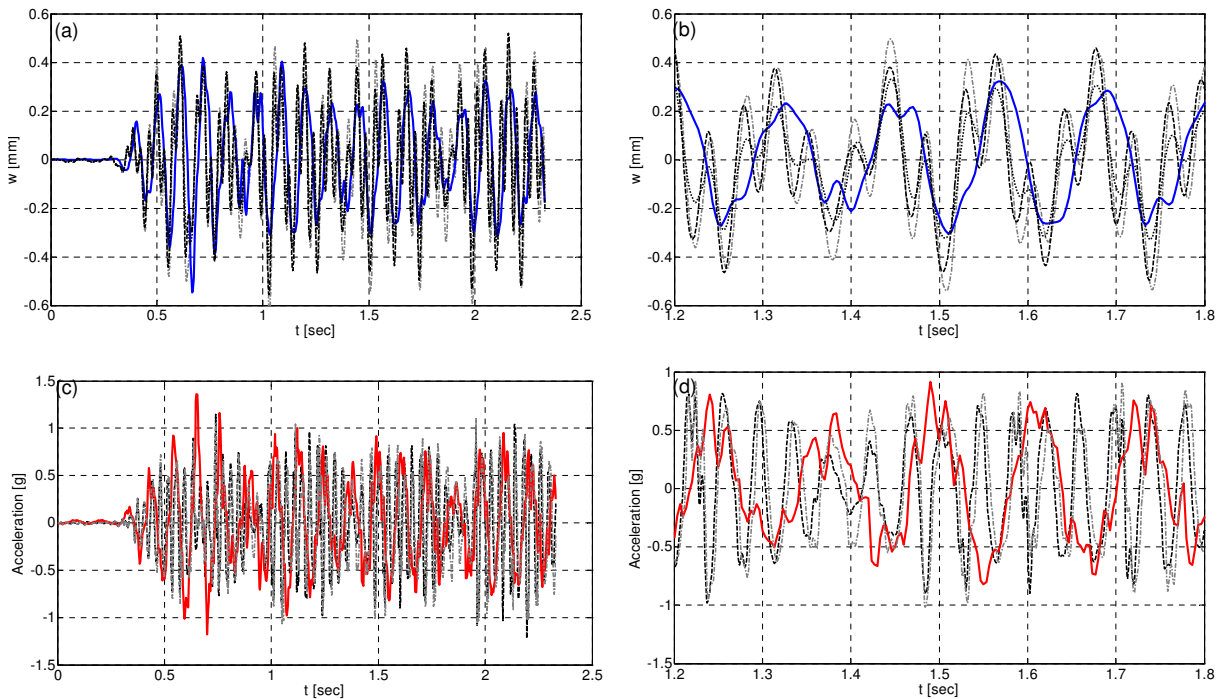


Figure 3. Dynamic response under higher level of vertical loading and out-of-plane excitation. (a) out-of-plane displacements at mid-height vs. time; (b) zoom on $t = 1.2$ – 1.8 sec; (c) out-of-plane accelerations at mid-height vs. time; (d) zoom on $t = 1.2$ – 1.8 sec. Legend: — = experimental; - - - = analysis, full-height model; - · - · - = analysis, refined symmetric model; ····· = analysis, higher damping ratio (Figure 3b only).

displacements which are about 1.5–1.8 times larger [Rabinovitch and Madah 2011]. The comparison between the numerical and the experimental results and between the two numerical models reveals a reasonable agreement, both in terms of amplitudes and in terms of the leading frequency of the temporal variation. On the other hand, it is observed that both numerical models tend to overestimate the effect of higher frequencies. The higher frequencies are noticeable in the experimental response, but they are less dominant.

A fast-Fourier-transform (FFT) analysis of the results reveals that the higher frequencies are detected in the range of about 21–28 Hz. This range corresponds to the first elastic natural frequency of the strengthened wall. The overestimation of the effect of the natural frequencies, which, in the present case, are higher than the frequency of the dynamic load, implies that the level of damping assumed in the analysis is probably underestimated. In order to examine this hypothesis, the results of the analysis with an exaggerated global damping ratio (20% of the critical one in the first two modes) appear in a dotted line in Figure 3b (for clarity of the figure, this line is not presented in Figure 3a). The results of the model with the higher level of damping reveal a less prominent effect of the higher frequencies and a better agreement with the experimental observations. This implies that the actual level of damping is higher than the one assumed in the original analysis. It should, however, be noted that the higher level of damping is also strongly affected by contributions of the test apparatus and, particularly, the lateral and vertical hydraulic loading systems. Yet, the observations regarding the effect of dissipation indicates that improvement of the simplified proportional damping model adopted in the analysis, its replacement with a more sophisticated damping model, and its calibration using the detailed experimental results are necessary directions of future enhancement of the analysis.

The comparison between the results of the full-height model and the symmetric one reveal that the amplitudes described by the latter are slightly higher than the ones detected by the former. This is attributed to the different representations of the self-weight of the wall in the two models, the a-symmetry that the self-weight introduces, and the a-symmetry in the in-plane configuration. Another contributor to the differences between the two models is the different representation of damping, which depends on the dynamic characteristics of each model.

The comparison in terms of accelerations appears in Figure 3c-d and reveals that the two numerical simulations and the experimental results are in agreement in terms of magnitude. Figure 3c also shows that the numerical model captures the slight beat effect observed in the experimental result. On the other hand, as expected, the effect of the higher frequency observed in the displacement response is more pronounced here. This effect further stresses the need to investigate the dissipative mechanisms in the wall as well as their implementation in the numerical model.

Another important aspect of the dynamic response is the temporal variation of the axial reaction at the top of the wall. These numerical and experimental results appear in Figure 4a-b. In this case, the presentation of the numerical results is limited to the symmetric model. The results refer to the 400 mm wide strip and include the weight of the loading devices located at the top of the wall. The comparison between the numerical and the experimental results reveals a good agreement in terms of the magnitude of the dynamic component of the thrust force. On the other hand, the analysis predicts a more rapid variation of the thrust force with frequency that is close to the first natural frequency of the wall in its intact condition. The frequency of the dynamic component detected in the experiment is closer to the one governing the forced excitation (about 8.3 Hz). Also here, the higher frequency response observed

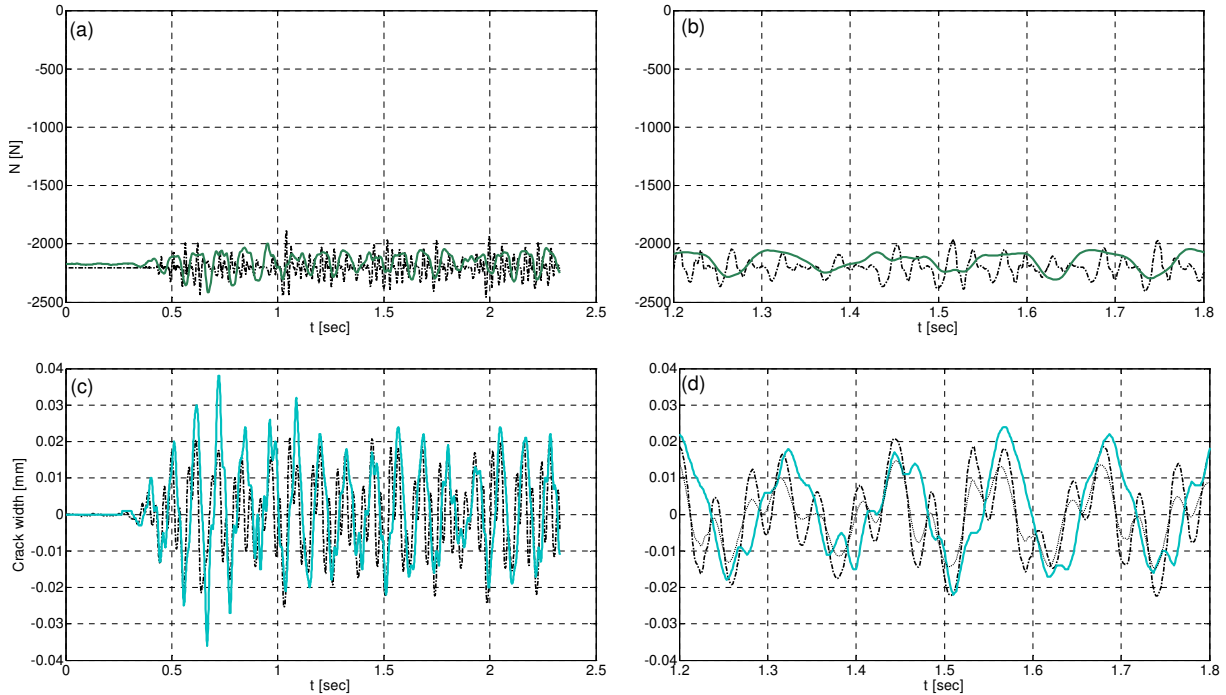


Figure 4. Dynamic response under higher level of vertical loading and out-of-plane excitation. (a) axial force at the top of the wall vs. time; (b) zoom on $t = 1.2\text{--}1.8$; (c) relative axial displacements across the middle joint (west face) versus time; (d) zoom on $t = 1.2\text{--}1.8$ sec. Legend: — = experimental; - - - = analysis, symmetric model; ····· = analysis, higher damping ratio (Figure 4d only).

in the analysis is attributed to underestimation of the damping and its effect on the out-of-plane response. On the other hand, the experimental observation reflects on coupling between the in-plane and the out-of-plane excitations. Such coupling, which may stem from imperfections in the test set-up, trigger auxiliary in-plane excitation of the wall with the same frequency as the out-of-plane one. This scenario, which can also explain the nonsymmetric or “nonsinusoidal” signal observed in the experimental results in Figure 4a-b, is not accounted for in the analysis.

The temporal variation of the axial deformations across the mid-height joint is studied in Figure 4c-d. In the experiment, the relative displacements are measured across two points located 90 and 120 mm above and below the center of the mid-height joint (LVDT2 in Figure 1). In the numerical analysis, the relative displacements are evaluated based on the reference axis displacements and rotations at these points. In both cases, the relative displacements due to the axial loading are not included and the presentation is limited to the results of the refined symmetric model, which provides a better description of the displacement field in the joint. The results appear in Figure 4c-d and indicate on a rather symmetric response with respect to the zero displacement line. This implies that under the examined conditions, the effect of shift of the axis of rotation (“neutral axis”) and the effect of rocking are not significant. The comparison between the numerical and the experimental results indicates that the analysis well captures the variation of the axial displacements across the joints. At the first second of the response, the analysis

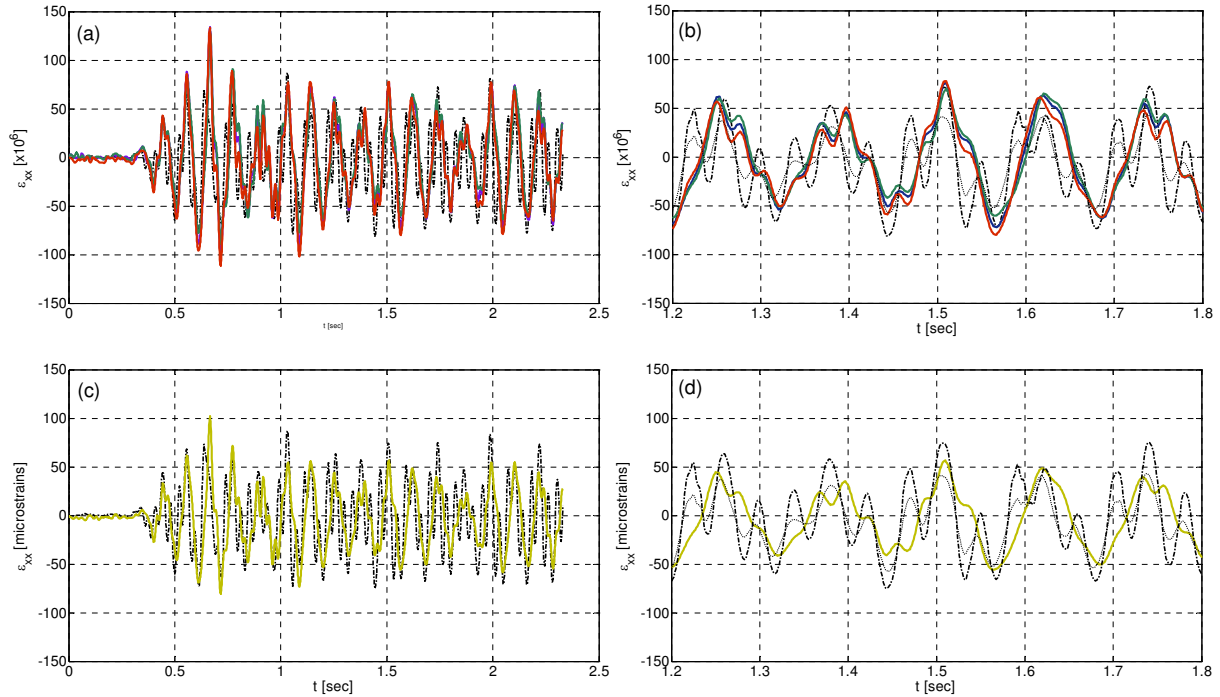


Figure 5. Strains at the outer face of the FRP strips versus time. (a) SG1,SG2, SG3 (middle of the joint) vs. time; (b) zoom plot $t = 1.2-1.8$ sec; (c) SG4 (30 mm above the middle joint-block interface, middle west strip); (d) zoom plot $t = 1.2-1.8$ sec. Legend: — SG1; — SG2 — SG3, — SG4 (experimental); - · - · - analysis, symmetric model, damping ratio=7%; · · · · · analysis, symmetric model, damping ratio=20%.

slightly overestimates the level of displacements. Later on, the discrepancies decay, revealing a good agreement in terms of amplitudes. The slight overestimation of the effect of the higher frequency by the numerical model decays with the increase in damping ratio.

A more refined class of results that focus on a more “localized” aspect of the dynamic response of the wall examines the strains at the outer face of the FRP strips near the mid-height joint. These results are studied in Figure 5. Note that here the zero lines refer to the initiation of the dynamic test and do not take into account the strains due to the vertical loading. The numerical results are presented for the symmetric model and they refer to the strain at the middle of the 5 mm long strain gauge.

The comparison between the strains measured at the outer faces of the middle of the joint at the left, middle, and right FRP strips (Figure 5a and zoom plot in Figure 5b) reveal only minor differences between the measured values. This supports the assumption that in spite of the running bond texture and the inhomogeneous structure of the masonry wall, the structure is governed by a clear unidirectional action. It also supports the modeling assumption that the analysis can focus on a characteristic strip composed of one course of masonry units and one FRP strip bonded on each side. The results of the numerical model are in good agreement with the experimental ones. The FE model well captures the magnitude of the strains and their temporal variation. The increased weight given by the model to the excitation of the higher frequency decays with the increase of the damping ratio (see the dotted lines).

Another interesting aspect is the variation of the strain state from the masonry unit region to the joint region. This aspect is governed by the stress transfer through the adhesive layer. In order to examine this effect, the strains at the outer face of the FRP strip at a point located 30 mm above the upper mortar-block interface of the mid-height joint are plotted in Figure 5c. A zoom plot appears in Figure 5d. The comparison of these results with the ones obtained for the same FRP strip but at the middle of the joint (Figure 5a-b) reveals the amplification of the strains in the joint region. As the joints represent the weaker, more compliant, and more brittle component of the masonry construction, the amplification is an outcome of the transfer of loads from the masonry units to the FRP strips. This is achieved by means shear and out-of-plane normal stresses in the adhesive layers. The comparison between the numerical and the experimental results reveals a good agreement both at the joint region (Figure 5a-b), and at the block region (Figure 5c-d). Although to a slightly smaller extent, the model also captures the reduction in strain (negative ones, mainly) away from the joint.

3.2. Complementary numerical results: higher level of vertical loading. The spatial and temporal distributions of the shear stresses in the adhesive layers appear in Figure 6a and 6b, respectively. The results are presented based on the analysis of the refined symmetric model. The distributions along the upper half of the wall (Figure 6a) reveal the localized peaks near the mortar joints and near the edge of the FRP system. These peaks are affected by the dynamic out-of-plane response, the initial compressive loading, the evolution of the compressive force in the wall, and the nonlinear behavior of the mortar material. Figure 6a indicates that in the present case, the stresses near the edges of the strip attain the largest values.

The variation in time of the peak shear stresses near the edge ($x = 205$ mm) and near the middle joint ($x = 1047.5$ mm) (points I–IV in Figure 6a) is studied in Figure 6b. The results reveal two different types of temporal behavior. The stresses near the edge are mostly affected by the global out-of-plane response as well as by the relatively high frequency response attributed by the numerical model to the axial compressive force (the thrust force). On the other hand, the temporal variation of the shear stresses near the inner joint (Figure 6b, III–IV) reveals that the base level of stresses due to the compressive loading is monotonically amplified at the initial stages of the dynamic response. The amplified level of

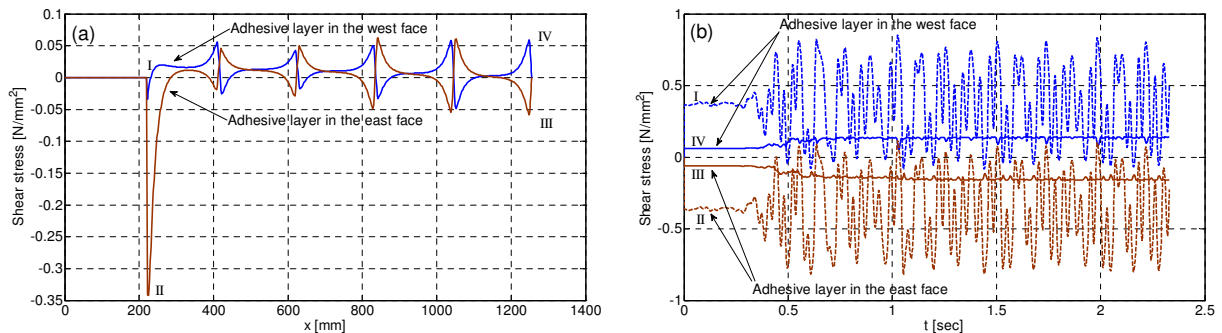


Figure 6. Spatial and temporal distributions of shear stresses in the adhesive layers. (a) distributions along the wall at $t = 1.56$ sec; (b) shear stresses at near the edge ($x = 205.0$ mm) and near the mid-height joint ($x = 1047.5$ mm) versus time. Legend: — stresses at $x = 205$ mm; - - - stresses at $x = 1047.5$ mm.

stress is less affected by the cyclic response revealing only a limited level of oscillations. This effect is attributed to the inelastic behavior of the mortar material and to the evolution of residual compressive strains in the mortar. Due to the inelastic behavior, the initiation of the dynamic load is associated with accumulation of compressive strains. As these compressive strains are inelastic by nature, they are not “released” during motion. Their evolution triggers the amplification of the shear stress at the first stages of the response. Later on, the steep unloading-reloading branch of the constitutive behavior of the mortar material dictates the high frequency oscillations and the pattern observed in Figure 6b.

The spatial and temporal variations of the out-of-plane normal stresses at the interfaces of the adhesive layer are studied in Figure 7. The spatial distributions reveal that in accordance with the shear stress concentration, the highest level of stresses is observed near the edge of the FRP strip. The temporal distributions reveal a notable oscillatory response that starts with the dynamic load. They also reveal that in both adhesive layers, the adhesive-masonry interface is mostly subjected to compressive normal stresses whereas the adhesive-FRP interface is mostly subjected to tension. The compressive stresses are amplified from a level of about 1.5 MPa under the vertical load to about 3.75 MPa under the dynamic excitation. The tensile stresses are also amplified by a similar ratio from about 0.5 MPa to about 1.35 MPa. These peeling stresses may trigger or accelerate a debonding failure. Furthermore, at certain points during the dynamic response, the compressive stresses that initially evolve at the critical adhesive-masonry

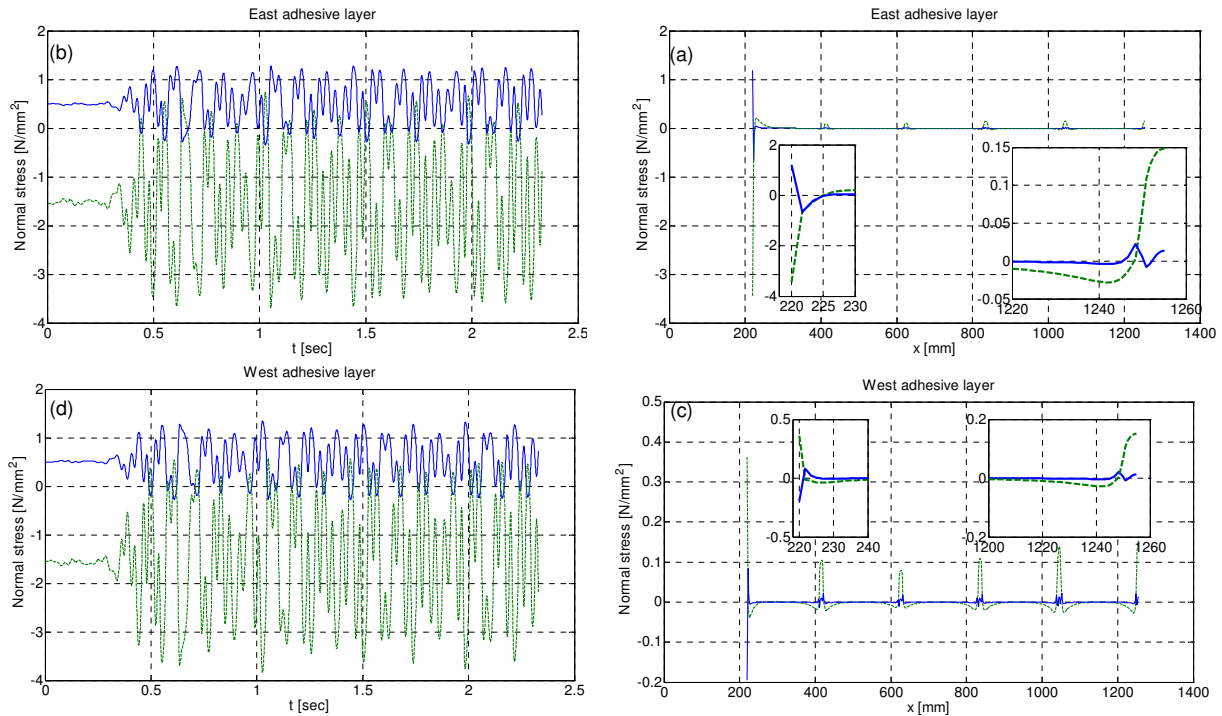


Figure 7. Spatial and temporal distributions of normal out-of-plane (peeling) stresses at the interface of the adhesive layers. (a) east layer, $t = 1.56$ sec; (b) east layer, $x = 1052.5$ mm; (c) west layer, $t = 1.56$ sec; (d) west layer, $x = 1052.5$ mm. Legend: — adhesive FRP interface; - - - adhesive-masonry interface.

interface turn into tensile stresses (see for example Figure 7c). At other points, both adhesive-masonry interfaces may be subjected to tension. These interfaces are usually brittle and governed by the limited ability of the masonry substrate to resist tensile stresses. Therefore, this unique condition, which evolves under the dynamic loading, may accelerate the evolution of dynamic debonding failure and may endanger the resilience of the strengthening system.

3.3. Test and analysis results: lower level of vertical loading. In this section, the results of a similar test conducted with a reduced level of vertical loading are studied. For comparison, the results for the wall before strengthening, which are discussed in detail in [Rabinovitch and Madah 2011], are also presented. It should be noted that in order to prevent total collapse, testing of the unstrengthened was terminated by shutting down the high power component of the hydraulic system after about 1.6 seconds. The results of both experiments are therefore presented for this limited period only. The out-of-plane accelerations and displacements in the strengthened and the original walls appear in Figure 8a-b. The temporal variations of the axial reaction at the top of the wall and the crack opening at the middle joint appear in Figure 8c-d.

The comparison between the original and the strengthened wall reveal significant differences and clearly point at the impact of the strengthening system. The response of the original wall is governed by

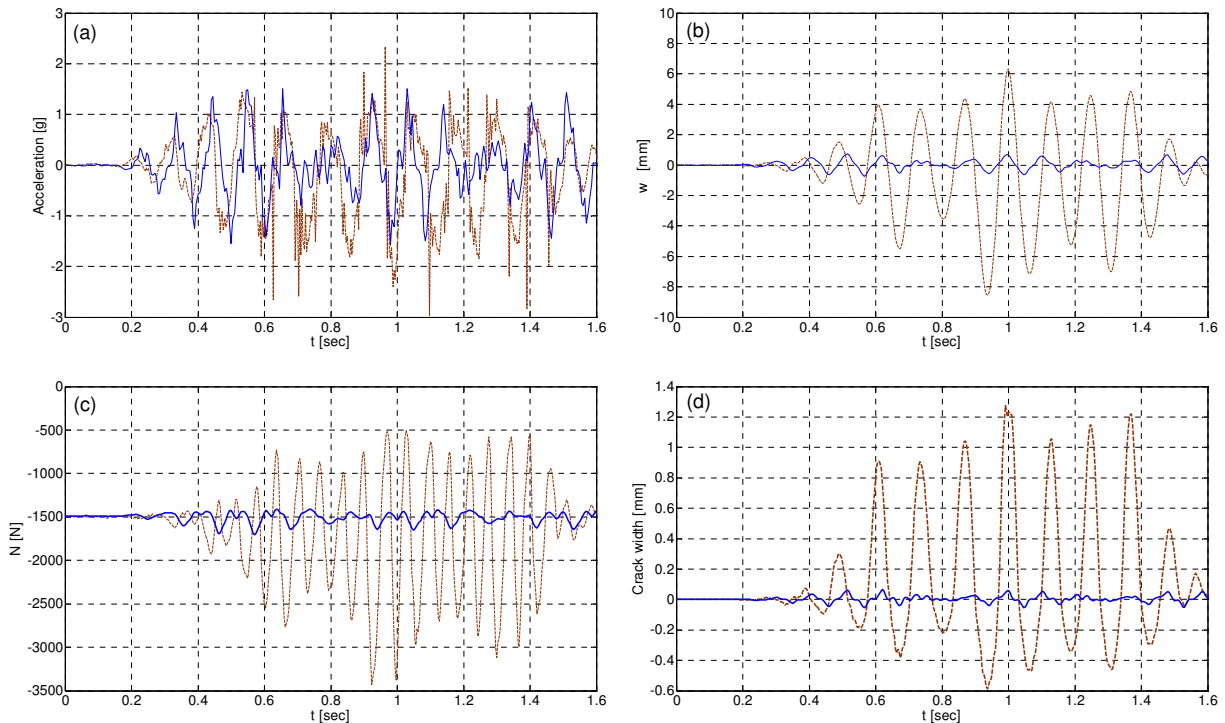


Figure 8. Dynamic response of strengthened and unstrengthened (original) walls under low level of vertical load and base excitation. (a) out-of-plane accelerations at mid-height; (b) out-of-plane displacements at mid-height; (c) axial reaction; (d) crack opening at mid-height. Legend: — strengthened wall; - - - unstrengthened wall. The results for the unstrengthened wall are adapted from [Rabinovitch and Madah 2011].

much larger out-of-plane displacement, extensive cracking at midspan, extensive rocking and variation of the axial compressive force in time, and possible relaxation of the rotational constraint at the top of the wall (see [Rabinovitch and Madah 2011] for more details). None of the above effects is observed in the response of the strengthened wall. The levels of out-of-plane displacements and crack opening observed in the strengthened wall are significantly smaller. The temporal variation of the thrust force, which is a direct outcome of the crack opening, the rocking, and the arching effects, is also notably smaller in the strengthened wall. These observations indicate that the strengthening system effectively and meaningfully changes the nature of the dynamic response of the masonry wall and significantly improves its ability to resist out-of-plane dynamic loads.

4. Summary and conclusions

The dynamic behavior of unidirectional strengthened masonry walls has been experimentally and numerically studied. This part of the paper has focused on shake-table testing of full-scale unidirectional FRP strengthened masonry wall subjected to different levels of axial loading and out-of-plane dynamic excitation. The results have revealed various aspects of the dynamic response including the global out-of-plane displacements and accelerations, the variation of the thrust force, and the variation of strains in the externally bonded reinforcement. It has also clearly showed that the application of the FRP reinforcement effectively changes the dynamic behavior of the masonry wall and drastically improves its ability to withstand significant out-of-plane dynamic loads.

The experimental results have also been used as reference for the examination of numerical results obtained using the finite element model developed in part I of this paper [Rabinovitch and Madah 2012]. The comparison in terms of out-of-plane displacements, in-plane displacements across the mid-height joint, and the strains at the outer face of the FRP layer have revealed good agreement and have provided some support and validation to the numerical model. On the other hand, the comparison has revealed that the model tends to overestimate the role of the natural frequency of the wall and to underestimate the effect of damping. This designates the incorporation of a refined and less general model for damping as a needed direction of further enhancement of the model.

Along with the experimental results and the comparison with the numerical ones, additional results in term of the stresses in the adhesive layer, their variation along the wall and from one interface to another, and their variation in time have been presented. This class of results, which cannot be directly deduced from experimental dynamic measurements, has thrown some light on the stress transfer between the wall and the supplemental layer and on the effect of the dynamic response on this mechanism. In particular, it has revealed the effect of the dynamic loading and the inelastic response of the mortar material on the evolution of interfacial shear and peeling stresses near the joints. These aspects may play a critical role in the potential initiation of dynamic debonding failures.

The experimental and numerical results have revealed and demonstrated the potential of the FRP bonding as an effective method for the dynamic upgrade of masonry walls. The ability of the strengthening system to significantly modify the dynamic response of the wall, to provide it with a load resisting mechanism, and to prevent its collapse under out-of-plane loads are critical steps towards the structural upgrade of masonry elements to resist dynamic loads. The ability of the numerical model to assess these effects is also an important step towards achieving this goal.

References

- [Al-Chaar and Hasan 2002] G. K. Al-Chaar and H. A. Hasan, "Dynamic response and seismic testing of CMU walls rehabilitated with composite material applied to only one side", *Proc. Inst. Civ. Eng. Struct. Build.* **152**:2 (2002), 135–146.
- [Albert et al. 2001] M. L. Albert, A. E. Elwi, and J. J. R. Cheng, "Strengthening of unreinforced masonry walls using FRPs", *J. Compos. Constr. (ASCE)* **5**:2 (2001), 76–84.
- [Almusallam and Al-Salloum 2007] T. H. Almusallam and Y. A. Al-Salloum, "Behavior of FRP strengthened infill walls under in-plane seismic loading", *J. Compos. Constr. (ASCE)* **11**:3 (2007), 308–318.
- [Altin et al. 2008] S. Altin, O. Anil, M. E. Kara, and M. Kaya, "An experimental study on strengthening of masonry infilled RC frames using diagonal CFRP strips", *Compos. B Eng.* **39**:4 (2008), 680–693.
- [Carpinteri and Pugno 2005] A. Carpinteri and N. Pugno, "Towards chaos in vibrating damaged structures, I: Theory and period doubling cascade", *J. Appl. Mech. (ASME)* **72**:4 (2005), 511–518.
- [Davidson et al. 2005] J. S. Davidson, J. W. Fisher, M. I. Hammons, J. R. Porter, and R. J. Dinan, "Failure mechanisms of polymer-reinforced concrete masonry walls subjected to blast", *J. Struct. Eng. (ASCE)* **131**:8 (2005), 1194–1205.
- [El-Dakhkhni et al. 2004] W. W. El-Dakhkhni, A. A. Hamid, and M. Elgaaly, "Seismic retrofit of concrete-masonry-infilled steel frames with glass-reinforced fiber polymer laminates", *J. Struct. Eng. (ASCE)* **130**:9 (2004), 1343–1352.
- [ElGawady et al. 2002] M. A. ElGawady, P. Lestuzzi, and M. Badoux, "Dynamic in-plane behavior of URM wall upgraded with composites", in *ICCI'02: Third International Conference on Composites in Infrastructure* (San Francisco, 2002), University of Arizona/Omnipress, Tucson, AZ, 2002.
- [ElGawady et al. 2003] M. A. ElGawady, P. Lestuzzi, and M. Badoux, "In-plane lateral behavior of URM walls upgraded with composites", in *Response of structures to extreme loading: proceedings of XL-2003* (Toronto, 2003), Elsevier, Boston, 2003.
- [Flanagan and Bennett 1999] R. D. Flanagan and R. M. Bennett, "Bidirectional behavior of structural clay tile infilled frames", *J. Struct. Eng. (ASCE)* **125**:3 (1999), 236–244.
- [Gilstrap and Dolan 1998] J. M. Gilstrap and C. W. Dolan, "Out-of-plane bending of FRP-reinforced masonry walls", *Compos. Sci. Technol.* **58**:8 (1998), 1277–1284.
- [Griffith et al. 2004] M. C. Griffith, N. T. K. Lam, J. L. Wilson, and K. Doherty, "Experimental investigation of unreinforced brick masonry walls in flexure", *J. Struct. Eng. (ASCE)* **130**:3 (2004), 423–432.
- [Hamed and Rabinovitch 2010a] E. Hamed and O. Rabinovitch, "Failure characteristics of FRP-strengthened masonry walls under out-of-plane loads", *Eng. Struct.* **32**:8 (2010), 2134–2145.
- [Hamed and Rabinovitch 2010b] E. Hamed and O. Rabinovitch, "Lateral out-of-plane strengthening of masonry walls with composite materials", *J. Compos. Constr. (ASCE)* **14**:4 (2010), 376–387.
- [Hamilton and Dolan 2001] H. R. Hamilton, III and C. W. Dolan, "Flexural capacity of glass FRP strengthened concrete masonry walls", *J. Compos. Constr. (ASCE)* **5**:3 (2001), 170–178.
- [Meisl et al. 2007] C. S. Meisl, K. J. Elwood, and C. E. Ventura, "Shake table tests on the out-of-plane response of unreinforced masonry walls", *Can. J. Civ. Eng.* **34**:11 (2007), 1381–1392.
- [Myers et al. 2004] J. J. Myers, A. Belarbi, and K. A. El-Domiati, "Blast resistance of FRP retrofitted un-reinforced masonry (URM) walls with and without arching action", *Masonry Soc. J.* **22**:1 (2004), 9–26.
- [Rabinovitch and Madah 2011] O. Rabinovitch and H. Madah, "Finite element modeling and shake-table testing of unidirectional infill masonry walls under out-of-plane dynamic loads", *Eng. Struct.* **33**:9 (2011), 2683–2696.
- [Rabinovitch and Madah 2012] O. Rabinovitch and H. Madah, "Dynamics of FRP strengthened unidirectional masonry walls, I: A multi-layered finite element", *J. Mech. Mater. Struct.* **7** (2012), 1–28.
- [Thompson and Stewart 1986] J. M. T. Thompson and H. B. Stewart, *Nonlinear dynamics and chaos: geometrical methods for engineers and scientists*, Wiley, Chichester, 1986.
- [Turek et al. 2007] M. Turek, C. E. Ventura, and S. Kuan, "In-plane shake-table testing of GFRP-strengthened concrete masonry walls", *Earthq. Spectra* **23**:1 (2007), 223–237.
- [Wu et al. 2005] C. Wu, H. Hao, and Y. Lu, "Dynamic response and damage analysis of masonry structures and masonry infilled RC frames to blast ground motion", *Eng. Struct.* **27**:3 (2005), 323–333.

Received 29 Aug 2010. Revised 9 Feb 2011. Accepted 10 Feb 2011.

ODED RABINOVITCH: cvoded@tx.technion.ac.il

Faculty of Civil and Environmental Engineering, Technion – Israel Institute of Technology, Haifa, 32000, Israel

HAZEM MADAH: hazem@tx.technion.ac.il

Faculty of Civil and Environmental Engineering, Technion – Israel Institute of Technology, Haifa, 32000, Israel

JOURNAL OF MECHANICS OF MATERIALS AND STRUCTURES

jomms.net

Founded by Charles R. Steele and Marie-Louise Steele

EDITORS

CHARLES R. STEELE Stanford University, USA
DAVIDE BIGONI University of Trento, Italy
IWONA JASIUK University of Illinois at Urbana-Champaign, USA
YASUhide SHINDO Tohoku University, Japan

EDITORIAL BOARD

H. D. BUI École Polytechnique, France
J. P. CARTER University of Sydney, Australia
R. M. CHRISTENSEN Stanford University, USA
G. M. L. GLADWELL University of Waterloo, Canada
D. H. HODGES Georgia Institute of Technology, USA
J. HUTCHINSON Harvard University, USA
C. HWU National Cheng Kung University, Taiwan
B. L. KARIHALOO University of Wales, UK
Y. Y. KIM Seoul National University, Republic of Korea
Z. MROZ Academy of Science, Poland
D. PAMPLONA Universidade Católica do Rio de Janeiro, Brazil
M. B. RUBIN Technion, Haifa, Israel
A. N. SHUPIKOV Ukrainian Academy of Sciences, Ukraine
T. TARNAI University Budapest, Hungary
F. Y. M. WAN University of California, Irvine, USA
P. WRIGGERS Universität Hannover, Germany
W. YANG Tsinghua University, China
F. ZIEGLER Technische Universität Wien, Austria

PRODUCTION contact@msp.org

SILVIO LEVY Scientific Editor

Cover design: Alex Scorpan

Cover photo: Ev Shafir

See <http://jomms.net> for submission guidelines.

JoMMS (ISSN 1559-3959) is published in 10 issues a year. The subscription price for 2012 is US \$555/year for the electronic version, and \$735/year (+\$60 shipping outside the US) for print and electronic. Subscriptions, requests for back issues, and changes of address should be sent to Mathematical Sciences Publishers, Department of Mathematics, University of California, Berkeley, CA 94720-3840.

JoMMS peer-review and production is managed by EditFLOW[®] from Mathematical Sciences Publishers.

PUBLISHED BY
 **mathematical sciences publishers**
<http://msp.org/>

A NON-PROFIT CORPORATION

Typeset in L^AT_EX

Copyright ©2012 by Mathematical Sciences Publishers

Journal of Mechanics of Materials and Structures

Volume 7, No. 1

January 2012

Dynamics of FRP strengthened unidirectional masonry walls I: A multilayered finite element	ODED RABINOVITCH and HAZEM MADAH	1
Dynamics of FRP strengthened unidirectional masonry walls II: Experiments and comparison	ODED RABINOVITCH and HAZEM MADAH	29
Peridynamic analysis of fiber-reinforced composite materials	ERKAN OTERKUS and ERDOGAN MADENCI	45
Postbuckling and delamination growth for delaminated piezoelectric elastoplastic laminated beams under hygrothermal conditions	YING-LI LI, YI-MING FU and HONG-LIANG DAI	85
Equivalent inhomogeneity method for evaluating the effective conductivities of isotropic particulate composites	SOFIA G. MOGILEVSKAYA, VOLODYMYR I. KUSHCH, OLESYA KOROTEEVA and STEVEN L. CROUCH	103



1559-3959(2012)7:1;1-D